JACS
JOURNAL OF THE AMERICAN CHEMICAL SOCIETY

Article

pubs.acs.org/JACS

Experimental and Theoretical Evaluation of Multisite Cadmium(II) Exchange in Designed Three-Stranded Coiled-Coil Peptides

Saumen Chakraborty,[†,∥] Olga Iranzo,[†,§] Erik R. P. Zuiderweg,*[,‡] and Vincent L. Pecoraro*[,†]

[†]Department of Chemistry, University of Michigan, and [‡]Department of Biological Chemistry, University of Michigan Medical School, Ann Arbor, Michigan 48109, United States

[§]Instituto de Tecnologia Química e Biológica, Universidade Nova de Lisboa, Avenida República, EAN 2781-901 Oeiras, Portugal

Supporting Information

ABSTRACT: An important factor that defines the toxicity of elements such as cadmium(II), mercury(II), and lead(II) with biological macromolecules is metal ion exchange dynamics. Intriguingly, little is known about the fundamental rates and mechanisms of metal ion exchange into proteins, especially helical bundles. Herein, we investigate the exchange kinetics of Cd(II) using *de novo* designed three-stranded coiled-coil peptides that contain metal complexing cysteine thiolates as a model for the incorporation of this ion into trimeric, parallel coiled coils. Peptides were designed containing both a single Cd(II) binding site, **Grand**-L12AL16C [**Grand** = AcG-$(LKALEEK)_5$-GNH_2], **Grand**L26AL30C, and **Grand**L26AE28QL30C, as well as **Grand**L12AL16CL26AL30C with two Cd(II) binding sites. The binding of Cd(II) to any of these sites is of high affinity ($K_A > 3 \times 10^7$ M^{-1}). Using ^{113}Cd NMR spectroscopy, Cd(II) binding to these designed peptides was monitored. While the Cd(II) binding is in extreme slow exchange regime without showing any chemical shift changes, incremental line broadening for the bound ^{113}Cd(II) signal is observed when excess ^{113}Cd(II) is titrated into the peptides. Most dramatically, for one site, L26AL30C, all ^{113}Cd(II) NMR signals disappear once a 1.7:1 ratio of Cd(II)/$(peptide)_3$ is reached. The observed processes are not compatible with a simple "free-bound" two-site exchange kinetics at any time regime. The experimental results can, however, be simulated in detail with a multisite binding model, which features additional Cd(II) binding site(s) which, once occupied, perturb the primary binding site. This model is expanded into differential equations for five-site NMR chemical exchange. The numerical integration of these equations exhibits progressive loss of the primary site NMR signal without a chemical shift change and with limited line broadening, in good agreement with the observed experimental data. The mathematical model is interpreted in molecular terms as representing binding of excess Cd(II) to surface Glu residues located at the helical interfaces. In the absence of Cd(II), the Glu residues stabilize the three-helical structure though salt bridge interactions with surface Lys residues. We hypothesize that Cd(II) interferes with these surface ion pairs, destabilizing the helical structure, and perturbing the primary Cd(II) binding site. This hypothesis is supported by the observation that the Cd(II)-excess line broadening is attenuated in **Grand**L26AE28QL30C, where a surface Glu(28), close to the metal binding site, was changed to Gln. The external binding site may function as an entry pathway for Cd(II) to find its internal binding site following a molecular rearrangement which may serve as a basis for our understanding of metal complexation, transport, and exchange in complex native systems containing α-helical bundles.

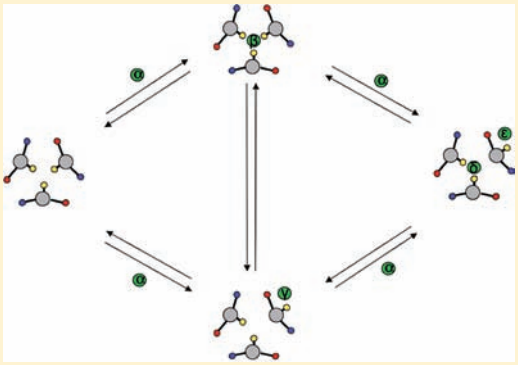

INTRODUCTION

Metal ion transport and homeostasis are critical cellular processes required for the maintenance of cellular health. One may distinguish two important classes of metal ion control. The first category addresses the proper handling of essential elements (e.g., Fe, Ni, Cu) in order to localize these metals in the appropriate protein, while minimizing the potential deleterious effects of the free ion. The second group contains the (usually) purely toxic ions (e.g., mercury(II), cadmium(II), arsenic(III), and lead(II)) which a cell encounters and which must be sequestered and detoxified before they are released back into the cellular environment. Nature often employs different strategies for uptake and transport of different essential metal ions. Some proteins such as albumin (binds Ca^{2+}, Na^+, K^+) or calmodulin (binds Ca^{2+}) sequester metals directly without any assistance by other proteins.[1,2] On the other hand, intracellular trafficking of transition metals such as copper and nickel occurs by the assistance of metallochaperone proteins, that are part of the cellular machinery which ensure that the proper metal ion is delivered to appropriate targets in a safe manner.[3−7] Remarkably, little is known about the fundamental rates and exchange

Received: November 8, 2011
Published: March 6, 2012

   dx.doi.org/10.1021/ja210510g | *J. Am. Chem. Soc.* 2012, 134, 6191−6203

pathways that control both the uptake and transport of metal ions by proteins into different cellular environments or different protein structure types.

Lower organisms such as bacteria, have evolved a detoxification mechanism to cope with heavy metals such as Hg(II), Cd(II), As(III), and Pb(II) by using different repressor proteins such as MerR,[8,9] CadC/CmtR,[10−13] ArsR/SmtB,[14] and pbrR.[15,16] In the absence of heavy metals these proteins bind to DNA, blocking the transcription of the genes that code for proteins that extrude heavy metals from cells. Upon metal binding the repressor protein either twists the DNA (MerR) or dissociates from DNA (CadC/CmtR, ArsR/SmtB) after undergoing a conformational change which then allow transcription to occur. In all of these cases, the proteins display exclusive Cys ligation around the metal centers, and in the SmtB class utilize helical domains for metal interaction. A fundamental understanding of heavy metal biochemistry requires a complete description of the metal's first coordination sphere and the corresponding physical properties that such a site confers. The rates for metal incorporation and removal are essential parts for proper functioning of metalloregulatory and metallochaperone proteins. However, complete understanding of the mechanistic pathways in which metals insert into, and are released from, metalloproteins are not well documented.[6,7,17−22] More specifically, the exchange rates for metal ion insertion into metalloregulatory proteins are not known and are of fundamental interest. Unfortunately, such information cannot be acquired by the study of small molecule systems and native proteins are often too complex to identify individual process critical for metal sequestration clearly.

Using a series of *de novo* parallel three-stranded coiled coils we have designed homoleptic thiol-rich binding sites for heavy metals such as Cd(II), Hg(II), Pb(II), and As(III) at the hydrophobic core of these polypeptides that has helped us clarify the heavy metal biochemistry of different metalloregulatory proteins. Following pioneering work by DeGrado and co-workers,[23] the *de novo* polypeptide systems are designed based on the general sequence Ac-G(LKALEEK)$_x$G-NH$_2$, where x is the number of heptad repeats.[24] Residues in positions 1 and 4 of the heptad form well-defined hydrophobic cores at the interior of the polypeptides. These peptides self-assemble in aqueous solution to form three-stranded coiled coils [Ac-G(LKALEEK)$_x$G-NH$_2$]$_3$, above pH 5.5.[25] These peptides provide us with simpler constructs for understanding more complicated native proteins. The successes using this strategy include the first spectroscopic and structural models[24,26−28] for Hg(II) binding to MerR, As(III) complexation[29,30] by ArsR, and trigonal[31] Cd(II) for CmtR. We have also demonstrated how to control the coordination geometry of metal ions such as Cd(II) at the peptide interior. Using a combination of ^{113}Cd NMR and ^{111m}Cd-perturbed angular correlation[32] (PAC) spectroscopies, it was shown that the peptide **Tri**L16C [**Tri** = Ac-G(LKALEEK)$_4$G-NH$_2$] bound Cd(II) as a mixture of three-coordinate trigonal planar CdS_3 and four-coordinate pseudotetrahedral CdS_3O (O = exogenous water molecule) species.[33] Removal of steric bulk directly above the metal binding site by replacing a Leu to an Ala led to the isolation of pure four-coordinate CdS_3O species in the peptide TriL12AL16C.[31,34] Pure three-coordinate CdS_3O geometry was achieved by increasing steric bulk in the first and second coordination sphere of the metal ion that blocked the access of the exogenous water molecule to the metal site, both employing unnatural amino acids. In the first strategy, metal binding Cys residues were replaced by bulky penicillamine (Pen, *gem*-dimethylcysteine) yielding the peptide **Tri**L16Pen.[31] In the second strategy, chirality of the Leu above the Cys site was modified by replacing L-Leu to D-Leu that caused the Leu side chains to orient toward the metal binding site (toward C-terminus of the bundle) which resulted in exclusive CdS_3 geometry in **Tri**L12L$_D$L16C.[35] Using this knowledge, heterochromic constructs **Grand**L16PenL26AL30C,[36] and **Grand**L12L$_D$L16CL26AL30C[35] [**Grand** = Ac-G(LKALEEK)$_5$-G-NH$_2$] were designed subsequently, each peptide containing both three- and four-coordinate sites which showed site-selective molecular recognition of Cd(II) for the four-coordinate CdS_3O geometry. Recently we have shown that depending on the topological position of the metal binding site (middle of the helix vs helical terminus) the physical properties of Cd(II) can be fine-tuned by the protein matrix even though the metal is bound as "identical" four-coordinate CdS_3O geometries at both the binding sites in the peptide **Grand**L12AL16CL26AL30C.[37]

In this study we have investigated the exchange dynamics associated with Cd(II) binding to various derivatives of GRAND series of peptides. Figure 1 shows a model of the three-stranded coiled coil. Clarification of the rules that we elucidate for encapsulation of heavy metals such as Cd(II), and the factors that influence these rates, should serve as the basis for our general understanding of heavy metal

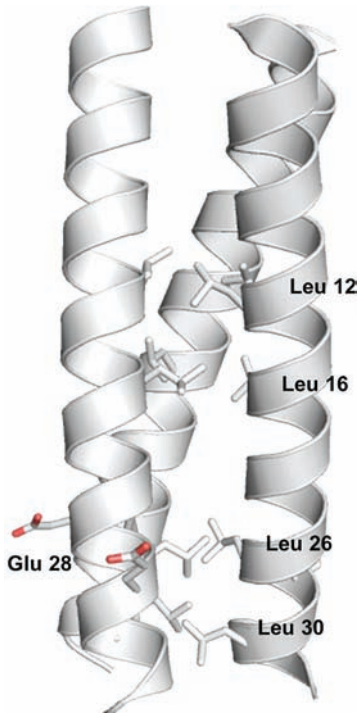

Figure 1. Model of the parallel three-stranded coiled-coil peptides investigated in this study. The model is derived on the basis of the X-ray structure of a related peptide, **CSL**9C (CS = Coil Ser) (PDB ID: 3LJM).[48] Peptide backbone is represented as gray cartoon, amino acid side chains that are modified yielding different derivatives of GRAND peptides (**Grand**L12AL16C, **Grand**L26AL30C, **Grand**L12AL16CL26AL30C, and **Grand**L26AE28QL30C) used in this study are shown as ball and stick representations. N→C terminus corresponds to top→bottom in this view parallel to the helical axis.

Table 1. Peptide Sequences Used in This Study[a]

Peptide	Sequence
	N- 1 9 16 23 30 37 -C
TRI	Ac-G LKALEEK LKALEEK LKALEEK LKALEEK G-NH_2
TriL9C	Ac-G LKALEEK CKALEEK LKALEEK LKALEEK G-NH_2
GRAND	Ac-G LKALEEK LKALEEK LKALEEK LKALEEK LKALEEK G-NH_2
GrandL26AL30C	Ac-G LKALEEK LKALEEK LKALEEK LKAAEEK CKALEEK G-NH_2
GrandL12AL16C	Ac-G LKALEEK LKAAEEK CKALEEK LKALEEK LKALEEK G-NH_2
GrandL26AE28QL30C	Ac-G LKALEEK LKALEEK LKALEEK LKAAEQK CKALEEK G-NH_2
GrandL12AL16CL26AL30C	Ac-G LKALEEK LKAAEEK CKALEEK LKALEEK CKALEEK G-NH_2
GrandL16PenL19IL23PenL26I	Ac-G LKALEEK LKALEEK XKAIEEK XKAIEEK LKALEEK G-NH_2

[a]X = penicillamine (Pen). Residues in red represent changes from the parent TRI or GRAND sequence. Sequences are shown as N- to C-terminus from left to right.

complexation and exchange processes in more complex systems such as metallochaperones, and metalloregulatory proteins such as CmtR and CadC which belong to the ArsR/SmtB metal sensing family which sense Cd(II) and Pb(II).[10,11]

Previous kinetic studies propose that Cd(II) insertion into three-stranded coiled coils follows a "breathing mechanism".[38] The assembly is thought to provide an opening for the metal by separation of two of the helices at the helical interface, in a slow and partially rate-determining step. Next, Cd(II) binds to the Cys residues at the interior of the coiled coil as a fast step with a concomitant loss of exogenous water molecule(s) bound to the metal ion. Subsequently, salt bridges that help stabilize the aggregate are reformed yielding the final metalated species. Here we are able to describe the breathing model in more detail. The insights are based on ^{113}Cd NMR studies using excess Cd(II) as compared to the primary binding site. The data are only compatible with a multisite exchange process that involves (several) surface sites that bind Cd(II) and destabilize the three-stranded coiled-coil structure. From this work, we also infer that surface glutamate residues play a crucial role in assisting the insertion of the metal ion from the helical interface to the primary metal binding site at the hydrophobic interior.

MATERIALS AND METHODS

Peptide Synthesis, Purification and Design Rationale. The GRAND peptides (see Table 1 for sequence nomenclature) were synthesized on an Applied Biosystems 433A peptide synthesizer using standard Fmoc protocols,[39] and purified and characterized as described previously.[40] Our initial ^{113}Cd(II) NMR titration experiments with **Grand**L12AL16C, where the CdS_3O metal binding site is located in the middle of the helical scaffold, suggested that an exchange process was occurring when excess metal was titrated. Next, experiments were performed with **Grand**L26AL30C, to see whether the metal site being located proximal to the C-terminus end of the bundle would show different exchange behavior than the L12AL16C site located in the middle of the helix. Subsequently, the peptide **Grand**L12AL16-CL26AL30C was studied to see whether the same sites (L12AL16C, L26AL30C) would show similar exchange properties, as was observed in individual peptides, when incorporated into a single peptide. The results from these experiments led us to hypothesize that there are additional surface binding sites (Glu) that are contributing to the exchange process. To test this hypothesis, we prepared **Grand**-L26AE28QL30C, where a surface Glu residue close to the primary metal binding site was changed to a non-metal-binding Gln. Finally, experiments were performed with the **Grand**L16PenL19IL23Pen-L26I peptide to see whether the three-coordinate CdS_3 sites also undergo exchange broadening like the four-coordinate CdS_3O sites under similar experimental conditions.

UV−Vis Spectroscopy. UV−vis spectroscopy was used to determine the stoichiometry and pH dependence of Cd(II) binding to the peptide **Grand**L26AE28QL30C. All solutions were purged with argon before use to minimize the chances of oxidation of the peptides and formation of disulfide bonds. Fresh stock solutions of the purified peptides were prepared for each experiment in doubly distilled water and their concentrations determined by quantization of the Cys thiol groups using a known assay with 4,4′-dipyridyl disulfide.[41]

Metal Binding Titrations. Titrations of Cd(II) into peptide were performed at room temperature on a Cary 100 Bio UV−vis spectrometer using a 1-cm quartz cuvette. Aliquots of 8.932 mM $CdCl_2$ stock solution were added into a 3-mL solution containing 60 μM peptide and 50 mM TRIS buffer at pH 8.5. In each case, the difference spectra were obtained by subtracting the background spectrum of the peptide in the absence of metal (60 μM peptide and 50 mM TRIS buffer at pH 8.5). The difference molar extinction coefficients ($\Delta\varepsilon$) are calculated based on the total metal concentration.

pH Titrations. UV−vis pH titrations were carried out at room temperature on an Ocean Optics SD 2000 fiber optic spectrometer and the pH measured using a mini-glass combination pH electrode (Hamilton Biotrode) coupled to a Fisher Accumet digital pH meter model 805 MP. pH titrations were performed by adding small aliquots of concentrated solution of KOH to unbuffered solutions containing $CdCl_2$ (20 μM) and peptide (60 μM), and monitoring the change in absorbance at 235 nm as a function of pH. Equilibration time was always allowed before reading the final pH. In all cases, reverse titrations were carried out by adding small aliquots of concentrated solution of HCl to verify the reversibility of the process. The UV−vis pH titration curve of the peptide **Grand**L26AE28QL30C was analyzed using the model and the fitting equation published previously for the simultaneous release of two Cys thiol protons upon formation of tristhiolato cadmium(II) species $(CdS_3)^-$ at high pH from a monothiolato cadmium(II) complex $(CdS(SH)_2)^+$ that exists at low pH.[42,43]

^{113}Cd NMR Spectroscopy. All the spectra were collected at room temperature on a Varian Inova 500 spectrometer (110.92 MHz for ^{113}Cd) equipped with a 5-mm broadband probe. ^{113}Cd NMR spectra were externally referenced to a 0.1 M $Cd(ClO_4)_2$ solution in D_2O. A spectral width of 847 ppm (93 897 Hz) was sampled using a 5.0 μs 90° pulse and 0.05 s acquisition time with no delay between scans. Samples were prepared under a flow of argon by dissolving 30−35 mg of the lyophilized and degassed peptides in 450−500 μL of 15% D_2O/H_2O solution. The peptide concentrations were determined by using the assay with 4,4′-dipyridyl disulfide,[41] and the concentrations range from 9 to 18 mM peptide, which corresponds to 3−6 mM three-stranded coiled coil. The final samples were prepared by the addition of the appropriate amount of 250 mM $^{113}Cd(NO_3)_2$ solution (prepared from 95% isotopically enriched ^{113}CdO obtained from Oak Ridge

dx.doi.org/10.1021/ja210510g | J. Am. Chem. Soc. 2012, 134, 6191−6203

National Laboratory) and the adjustment of the pH with KOH or HCl solutions. The pH value was measured both before and after the experiment. An argon atmosphere was maintained when possible but the samples came in contact with air during addition of $^{113}Cd(NO_3)_2$, pH adjustment, and acquisition. The data were analyzed using the software MestRe-C.[44] All free induction decays (FIDs) were zero-filled to double the original points and were processed by application of 100 Hz line broadening prior to Fourier transformation.

Line Fitting Analysis of the ^{113}Cd NMR Spectra. Line fitting analysis of the ^{113}Cd NMR peaks was performed using the software MestRe-C by first defining the region of the spectra to be analyzed followed by selecting the peak of interest. Fittings were performed by keeping the chemical shift and the intensity of the peaks fixed while varying the line width (LW) of the peak during the iterative fitting process. The ratio of Lorentzian/Gaussian functions for each peak was kept constant at 1 (L/G = 1) during the fitting analysis.

Two-Site Exchange Kinetics Modeling. The fractions of the species as a function of total Cd(II) and total protein concentration were obtained from numerical integrations of simple binding kinetics equations. While this simple case has an analytical solution (the well-known quadratic equation), we used numerical integration because it was needed for the subsequent more complicated binding simulations and served as a test-bed. The equations used were

$$\begin{aligned}\frac{d[P]}{dt} &= -k_{on}[Cd][P] + k_{off}[P{\cdot}Cd]\\ \frac{d[Cd]}{dt} &= -k_{on}[Cd][P] + k_{off}[P{\cdot}Cd]\\ \frac{d[P{\cdot}Cd]}{dt} &= +k_{on}[Cd][P] - k_{off}[P{\cdot}Cd]\end{aligned} \quad (1)$$

with the starting conditions

$$\begin{aligned}[P]_{t=0} &= [P]_{total}\\ [Cd]_{t=0} &= [Cd]_{total}\\ [P{\cdot}Cd]_{t=0} &= 0\end{aligned} \quad (2)$$

The integrations were allowed to reach equilibrium ($t_{kin} = \infty$) The details of chemical shift and line width changes of two-site chemical exchange in the slow/intermediate regime, were obtained from numerical integrations of the Bloch–McConnell (BMC) equations,[45] which are valid for all time regimes without any approximations:

$$\begin{aligned}\frac{dM_x^{free}}{dt} &= -\omega_{free}M_y^{free} - R_2^{free}M_x^{free} - \tau_{free}^{-1}M_x^{free} + \tau_{bound}^{-1}M_x^{bound}\\ \frac{dM_y^{free}}{dt} &= +\omega_{free}M_x^{free} - R_2^{free}M_y^{free} - \tau_{free}^{-1}M_y^{free} + \tau_{bound}^{-1}M_y^{bound}\\ \frac{dM_x^{bound}}{dt} &= -\omega_{bound}M_y^{bound} - R_2^{bound}M_x^{bound} + \tau_{free}^{-1}M_x^{free} - \tau_{bound}^{-1}M_x^{bound}\\ \frac{dM_y^{bound}}{dt} &= +\omega_{bound}M_x^{bound} - R_2^{bound}M_y^{bound} + \tau_{free}^{-1}M_y^{free} - \tau_{bound}^{-1}M_y^{bound}\end{aligned} \quad (3)$$

The variables in the BMC equations are related to the variables in the kinetic eqs 1 as follows:

$$\begin{aligned}M_x^{free}(t_{BMC} = 0) &= [Cd](t_{kin} = \infty)\\ M_x^{bound}(t_{BMC} = 0) &= [P{\cdot}Cd](t_{kin} = \infty)\\ \tau_{bound}^{-1} &= k_{off}\\ \tau_{free}^{-1} &= k_{on}[P](t_{kin} = \infty)\\ M_y^{free}(t_{BMC} = 0) &= 0\\ M_y^{bound}(t_{BMC} = 0) &= 0\end{aligned} \quad (4)$$

The FIDS were computed until the signal had decayed to <0.01 of the starting signal. NMR spectra such as those shown in Figure 3 in the Discussion were obtained by Fourier transformation of the calculated FIDs.

Five-Site Exchange Kinetics Modeling. A model for the binding of Cd(II) to one of the sites of a **Grand** peptide is shown in Figure 4 in the Discussion. In order to obtain quantitative estimations of the behavior of the scheme, we solved for the fractions of species at several different total Cd(II) concentrations by numerical integration of the kinetic eqs 5 until equilibrium is reached.

$$\begin{aligned}\frac{d[P]}{dt} &= -k_{PQ}[P][Cd] - k_{PR}[P][Cd] + k_{QP}[Q] + k_{RP}[R]\\ \frac{d[Q]}{dt} &= -k_{QS}[Q][Cd] - k_{QP}[Q] - k_{QR}[Q] + k_{PQ}[P][Cd] + k_{SQ}[S] + k_{RQ}[R]\\ \frac{d[R]}{dt} &= -k_{RS}[R][Cd] - k_{RP}[R] - k_{RQ}[R] + k_{PR}[P][Cd] + k_{SR}[S] + k_{QR}[Q]\\ \frac{d[S]}{dt} &= -k_{SQ}[S] - k_{SR}[S] + k_{QS}[Q][Cd] + k_{RS}[R][Cd]\\ \frac{d[Cd]}{dt} &= -k_{PQ}[P][Cd] - k_{PR}[P][Cd] - k_{QS}[Q][Cd] - k_{RS}[R][Cd] + k_{QP}[Q] + k_{RP}[R] + k_{SQ}[S] + k_{SR}[S]\end{aligned} \quad (5)$$

The initial free Cd(II) and free protein concentrations correspond to the known total Cd(II) and total protein concentrations, respectively, with all other initial concentrations set to zero:

$$\begin{aligned}[Cd]_{t=0} &= [Cd]_{total}\\ [P]_{t=0} &= [P]_{total}\\ [Q]_{t=0} &= 0\\ [R]_{t=0} &= 0\\ [S]_{t=0} &= 0\end{aligned} \quad (6)$$

These kinetic calculations were carried out for a variety of starting conditions. An example is shown in Figure S9 of the Supporting Information (SI). The obtained steady-state (equilibrium) concentrations as a function of total concentrations describe the sought-after description of the thermodynamics of the scheme as shown in Figure 5 in the Discussion. The scheme was then extended to incorporate NMR line-broadening effects due to kinetic effects. For the ^{113}Cd signal, the scheme in Figure 4 corresponds to a five-site exchange. Free Cd(II) in solution is designated as "site" α. Other possible sites where Cd(II) can bind are to the site β in species Q, to site γ in species R, or to sites δ or ε in species S. The relevant kinetic parameters are summarized in Figure 6. The effects of exchange kinetics on NMR relaxation is described by BMC equations,[45] which for a generic five-site exchange scheme are shown in eq 7,

$$\frac{\mathrm{d}}{\mathrm{d}t}\begin{bmatrix} M_\alpha^+ \\ M_\beta^+ \\ M_\gamma^+ \\ M_\delta^+ \\ M_\varepsilon^+ \end{bmatrix} = \begin{bmatrix} i\omega_\alpha - R_2^\alpha - \sum_{j\neq\alpha} r_{\alpha j} & r_{\beta\alpha} & r_{\gamma\alpha} & r_{\delta\alpha} & r_{\varepsilon\alpha} \\ r_{\alpha\beta} & i\omega_\beta - R_2^\beta - \sum_{j\neq\beta} r_{\beta j} & r_{\gamma\beta} & r_{\delta\beta} & r_{\varepsilon\beta} \\ r_{\alpha\gamma} & r_{\beta\gamma} & i\omega_\gamma - R_2^\gamma - \sum_{j\neq\gamma} r_{\gamma j} & r_{\delta\gamma} & r_{\varepsilon\gamma} \\ r_{\alpha\delta} & r_{\beta\delta} & r_{\gamma\delta} & i\omega_\delta - R_2^\delta - \sum_{j\neq\delta} r_{\delta j} & r_{\varepsilon\delta} \\ r_{\alpha\varepsilon} & r_{\beta\varepsilon} & r_{\gamma\varepsilon} & r_{\delta\varepsilon} & i\omega_\varepsilon - R_2^\varepsilon - \sum_{j\neq\varepsilon} r_{\varepsilon j} \end{bmatrix} \times \begin{bmatrix} M_\alpha^+ \\ M_\beta^+ \\ M_\gamma^+ \\ M_\delta^+ \\ M_\varepsilon^+ \end{bmatrix} \quad (7)$$

$$\begin{bmatrix} -(k_{int}+k_{ext})[P] - k_{int}[R] - k_{ext}[Q] & k_{QP} & k_{RP} & k_{SR} & k_{SQ} \\ k_{int}[P] & -k_{QP} - k_{QR} - k_{ext}[Cd] & k_{RQ} & k_{SQ} & 0 \\ k_{ext}[P] & k_{QR} & -k_{RP} - k_{RQ} - k_{int}[Cd] & 0 & k_{SR} \\ k_{int}[R] & k_{ext}[Cd] & 0 & -k_{SR} - k_{SQ} & 0 \\ k_{ext}[Q] & 0 & k_{int}[Cd] & 0 & -k_{SQ} - k_{SR} \end{bmatrix} \quad (8)$$

where M_j^+ are the complex coherences $M_j^x + iM_j^y$ of species j, ω_j the angular NMR frequencies in the different sites j, and R_2^j the intrinsic transverse relaxation rates of sites j. This generic scheme was adapted to the thermodynamic/kinetic scheme in Figure 6 in the Discussion by the substitutions shown in eq 8 for the non-NMR parameters in the kinetic matrix, where the concentrations of the species Cd, P, Q, R, and S were taken from the end points of the integrations of eq 5. The equilibrium concentrations obtained from the computations with eq 5 were used as starting conditions:

$$M_\alpha^+(0) = ([Cd], 0)$$
$$M_\beta^+(0) = ([Q], 0)$$
$$M_\gamma^+(0) = ([R], 0)$$
$$M_\delta^+(0) = ([S], 0)$$
$$M_\varepsilon^+(0) = ([S], 0) \quad (9)$$

Equations 8 were solved for different equilibrium conditions (obtained from eq 5) by numerical integration to obtain the different coherences as a function of time, i.e., to obtain the FIDS of all species. The FIDS were co-added, zero-filled, and transformed using a complex Fourier transform to obtain the spectra as shown in Figure 7 in the Discussion. All programs were written in Fortran-90, compiled using GNU compilers and executed using a 2.4 GHz Intel Core 2 Duo Apple MacbookPro running MacOS10.6.8.

RESULTS

UV−Vis Spectroscopy. Results from UV−vis spectroscopy can be found in the SI.

^{113}Cd NMR Spectroscopy. The Cd(II) binding to the peptide **Grand**L12AL16C, which has been shown to bind one Cd(II) ion with a four-coordinate CdS_3O geometry,[36] was investigated by ^{113}Cd NMR. The NMR spectrum shows a resonance at 572 ppm in the presence of 1.0 equiv of ^{113}Cd(II) (Figure 2A). When 1.5 equiv of ^{113}Cd(II) was added, the peak was slightly broadened, with no change in the chemical shift, indicating slow/intermediate exchange. The resonance further broadened and decreased in intensity in the presence of 2.0 equiv of ^{113}Cd(II) (Figure S3 of the SI shows fittings of the NMR spectra used to obtain the line widths). However, in the presence of excess Cd(II) no additional resonance was observed which could be attributed to the free ^{113}Cd(II), expected to appear in the upfield region between 0 and 100 ppm (see Figure S4 of the SI for the full chemical shift scale).[46]

After the initial observations with the **Grand**L12AL16C peptide, a careful stepwise titration was performed with the peptide **Grand**L26AL30C, which also binds one Cd(II) ion in CdS_3O geometry.[36] Addition of 0.2−0.8 equiv of ^{113}Cd-(II) to a solution containing 4 mM (**Grand**L26AL30C)$_3$ at

dx.doi.org/10.1021/ja210510g | J. Am. Chem. Soc. 2012, 134, 6191−6203

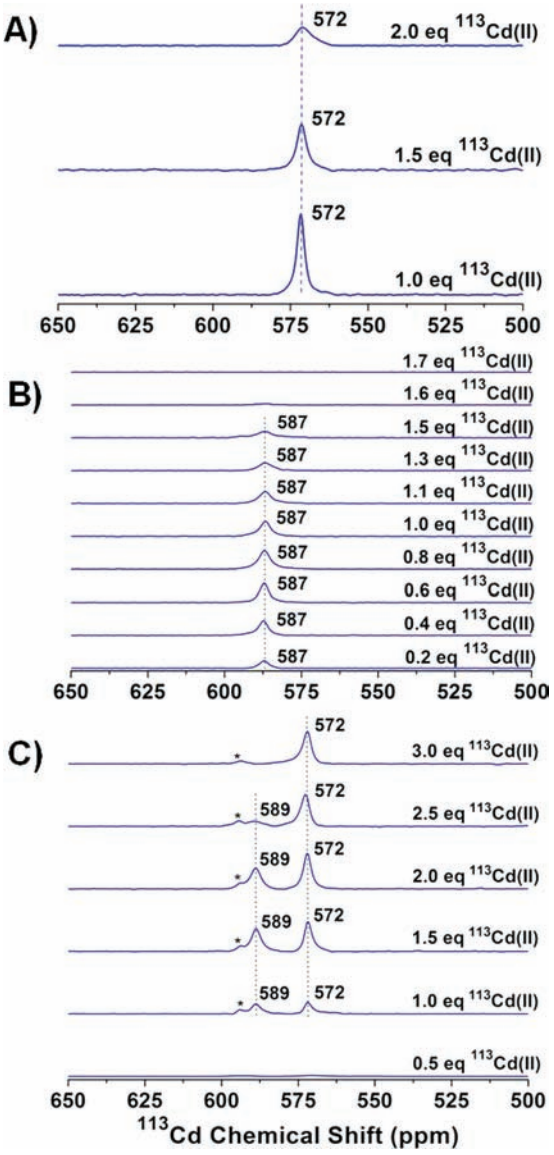

Figure 2. ^{113}Cd NMR spectra of solutions containing (A) 3.2 mM (**Grand**L12AL16C)$_3$ (the metal binding site located almost in the middle of the peptide) at pH 8.5 in the presence of 1.0, 1.5, and 2.0 equiv of ^{113}Cd(NO$_3$)$_2$, (B) 4.0 mM (**Grand**L26AL30C)$_3$ (the metal site located almost at the end of the peptide) at pH 8.5 in the presence of 0.2−1.7 equiv of ^{113}Cd(NO$_3$)$_2$, and (C) 3.2 mM (**Grand**L12AL16CL26AL30C)$_3$ (two metal binding sites, located in the middle and at the helical terminus of the peptide, respectively) at pH 8.5 with different equivalents of added ^{113}Cd(NO$_3$)$_2$. The most downfield peak marked with a star in (C) is an impurity most likely in the form of a peptide of shorter length that is produced during automated peptide synthesis and is inseparable by HPLC.

pH 8.5 led to a gradual increase in the intensity of the ^{113}Cd NMR resonance with a chemical shift of 587 ppm, while no line broadening of the peak was observed (Figure 2B). When 1.0 equiv of ^{113}Cd(II) was added, the peak slightly decreased in intensity, but no broadening was observed. With the gradual addition of more than 1.0 equiv of ^{113}Cd(II), the resonance at 587 ppm decreased in intensity and subsequently broadened. In the presence of 1.7 equiv of ^{113}Cd(II), the resonance had broadened beyond detection (Figure 2B). The line widths as measured from the spectra (see Figure S5 of the SI) are listed in Table 2. The resonance at 587 ppm did not shift during the course of ^{113}Cd(II) addition, showing that exchange is occurring on the slow/intermediate exchange regime. Again, in the presence of excess Cd(II) no additional resonance was observed which could be attributed to the free ^{113}Cd(II) (Figure S6 of the SI shows the full chemical shift scale). The comparison of these two results shows that the metal binding sites in the **Grand**L12AL16C and **Grand**L26AL30C peptides have different properties.

Table 2. ^{113}Cd NMR Frequencies and Line Widths for the Bound ^{113}Cd(II) Signal[a]

peptide	added Cd (equiv)	LW (Hz)
GrandL12AL16C	1.0	309
	1.5	393
	2.0	608
GrandL26AL30C	0.2	368
	0.4	420
	0.6	377
	0.8	411
	1.0	422
	1.1	470
	1.2	538
	1.3	570
	1.4	606
	1.5	634
GrandL12AL16CL26AL30C	1	308 (572 ppm site)
		422 (589 ppm site)
	1.5	287 (572 ppm site)
		391 (589 ppm site)
	2	303 (572 ppm site)
		381 (589 ppm site)
	2.5	343 (572 ppm site)
		472 (589 ppm site)
	3.0	348 (572 ppm site)
GrandL26AE28QL30C	1.0	378
	1.1	407
	1.2	401
	1.3	413
	1.4	518
	1.5	524
	2.0	737

[a]Base frequency: 111 MHz (500 MHz ^{1}H). The shifts were externally referenced to a 0.1 M Cd(ClO$_4$)$_2$ solution in D$_2$O.

We next investigated by NMR the peptide **Grand**L12AL16CL26AL30C to assess whether these two binding sites when incorporated into a *single* peptide have different properties. Furthermore, we examined whether placing two metal binding sites in the same peptide (**Grand**L12AL16CL26AL30C) alters the properties of the metal bound states when compared to the peptides containing a single metal binding site (**Grand**L12AL16C and **Grand**L26AL30C). **Grand**L12AL16CL26AL30C binds Cd(II) ions as four-coordinate pseudo-tetrahedral CdS$_3$O species at both metal binding sites (16 and 30 positions).[37] Gradual addition of 0.5 equiv of ^{113}Cd(II) to a solution containing 3.2 mM (**Grand**L12AL16CL26AL30C)$_3$ at

dx.doi.org/10.1021/ja210510g | J. Am. Chem. Soc. 2012, 134, 6191−6203

pH 8.5 led to an increase in intensity of the ^{113}Cd NMR resonances at 572 and 589 ppm up to 2.0 equiv of ^{113}Cd(II) (Figure 2C) (the most downfield peak marked with a star is an impurity from a peptide of shorter length that is produced during automated peptide synthesis and is inseparable by HPLC). The signals at 572 and 589 ppm correspond to chemical shifts of Cd(II) in the L12AL16C and L26AL30C sites, respectively.[37] In the presence of 2.0 equiv (stoichiometric) of ^{113}Cd(II), the two peaks gained full intensity. Adding an additional 0.5 equiv of ^{113}Cd(II) (2.5 equiv total) resulted in a significant decrease in intensity and broadening of the peak at 589 ppm. This observation is similar to the results obtained for the single site peptide **Grand**L26AL30C. The peak at 572 ppm underwent only a slight decrease in intensity and increase in broadening in the presence of 2.5 equiv of ^{113}Cd(II). None of the peaks shifted their respective resonance frequencies, indicating that the process is occurring on the slow exchange regime of the NMR time scale. When 3.0 equiv of ^{113}Cd(II) were added, the peak at 589 ppm had broadened beyond detection. The 572 ppm peak, on the other hand, was still present and did not broaden or lose further intensity. The line widths as measured from the spectra (see Figure S7 of the SI) are listed in Table 2. Again, in the presence of excess Cd(II) no additional resonance was observed which could be attributed to the free ^{113}Cd(II). These results show that the two metal binding sites in **Grand**L12AL16CL26AL30C have different properties from each other, but that each site appears to behave similarly to that observed for the single site peptides (e.g., L12AL16C sites in **Grand**L12AL16CL26AL30C and **Grand**-L12AL16C behave the same). This later observation demonstrates that adding a second metal binding site (at least 14 residues away) to either **Grand**L12AL16C or **Grand**L26AL30C does not cause significant perturbation to the metal ion bound at the original site.

DISCUSSION

The aim of this work is to describe at a molecular level how metal ions insert into helical scaffolds using *de novo* designed three-stranded coiled-coil peptides as model systems with the long-term objective of better understanding of metal exchange processes into more complex metalloproteins. The specific questions relating to Cd(II) exchange that are being addressed in this study are the following: Does the Cd(II) initially coordinate to any of the amino acids located at the surface of the peptide? Do the cysteine residues at the designed metal binding site play any role in internalizing the surface-bound Cd(II)? Does the exchange rate depend on the location of the metal binding site within the three-stranded coiled-coil interior (middle of the helix vs toward the helical terminus)? Can one site fine-tune the exchange behavior of a distant second metal site within the same peptide? And, is there any difference in the exchange behavior of the four-coordinate CdS_3O vs three-coordinate CdS_3 structure?

Effect of Peptide Design on the Properties of Cadmium(II) Binding. UV−vis spectroscopy shows that both peptides **Grand**L12AL16C and **Grand**L26AL30C bind Cd(II) with high affinity (see Figure S1 of the SI) ($K_A > 3 \times 10^7$ M^{-1}). PAC spectroscopy shows that the Cd(II) ions are encapsulated in a pseudotetrahedral CdS_3O geometry.[37,43] While no three-dimensional structure is as of yet available for these complexes, it has been assumed that the peptides are parallel triple-helical coiled coils in which three cysteines, one from each strand of the peptide, and an internal water molecule, bound along the helical axis, serve as ligands to the metal ion. The NMR spectra in Figure 2A,B are in agreement with these results. The chemical shifts at 572 and 587 ppm for **Grand**L12AL16C and **Grand**L26AL30C, respectively, correspond to a pseudotetrahedral CdS_3O environment, and the chemical shifts of the sites are not very different. Moreover, both binding sites show slow exchange characteristics, in agreement with the tight binding seen by UV−vis spectroscopy. The combined results would, therefore, suggest that the designed Cd(II) binding sites in **Grand**L12AL16C and **Grand**L26AL30C are very similar. However, when excess Cd(II) is added, the NMR data reveal significant differences between the sites: the bound Cd(II) resonance for **Grand**-L12AL16C remains visible when excess Cd(II) is present (Figure 2A), whereas the bound Cd(II) resonance for **Grand**L26AL30C disappears when similar amount of excess Cd(II) is present (Figure 2B). As will be discussed in detail below, these differences can, in rather involved ways, be attributed to differences in the kinetics of Cd(II) binding and release. Here, however, it suffices to establish that while the binding site affinities and coordination characteristics are independent of the location of the binding site in the peptide, the binding/release kinetics of these sites is not.

The results in Figure 2C indicate that the site-specific similarities and differences of the two single site peptides are retained in the dual-site peptide **Grand**L12AL16CL26AL30C. First, the ^{113}Cd chemical shifts at 572 and 589 ppm are almost identical to those seen in the peptides with the individual binding sites. Using a combination of ^{113}Cd NMR and ^{1}H−^{1}H NOESY spectroscopies,[37] we confirmed that the 589 ppm resonance in **Grand**L12AL16CL26AL30C indeed belongs to the L26AL30C site and the 572 resonance to the L12AL16C site. The correspondences of the ^{113}Cd shifts in the different peptides strongly suggest that there is no communication between these sites. Second, the difference in kinetic behavior of the two sites as seen in the individual single-site peptides is also maintained in **Grand**L12AL16CL26AL30C: the results in Figure 2C clearly show that site L26AL30C is more dynamic than site L12AL16C. Combined, these results indicate that the L26AL30C site, which is located close to the C-terminal end of the three-stranded coiled coil, is more susceptible to exchange of Cd(II) as compared to the L12AL16C site which is located almost in the middle of the helical scaffold. Due to its location, the L26AL30C site is more exposed to the bulk solvent since the α helices are subject to significant fraying.[30,47−49] These results, therefore, demonstrate that even though both the L12AL16C and L26AL30C sites in the **Grand**L12AL16-CL26AL30C peptide bind Cd(II) in "identical" first coordination sphere geometries (four-coordinate CdS_3O), the L26AL30C site is kinetically more labile. For **Grand**L12AL16CL26AL30C, one may also conclude that the sites do not affect each other's thermodynamic and kinetic properties.

Exchange Processes in ^{113}Cd(II) NMR Spectroscopy: Formulation of Two-Site Exchange Modeling and Its Implications. According to solid state NMR results, the aqueous ^{113}Cd(II) NMR signal is expected to occur around 50−100 ppm relative to $^{113}Cd(ClO_4)_2$, depending on counterions and ionic strength.[46] However, in practice, the NMR signal of ^{113}Cd(II) is difficult to detect in aqueous solution. This is likely due to broadening caused by the sizable ^{113}Cd(II) chemical shift anisotropy (CSA) relaxation.[50] This may be exacerbated by exchange broadening caused by dynamic rearrangement of the hydration shell. In contrast, all peptides

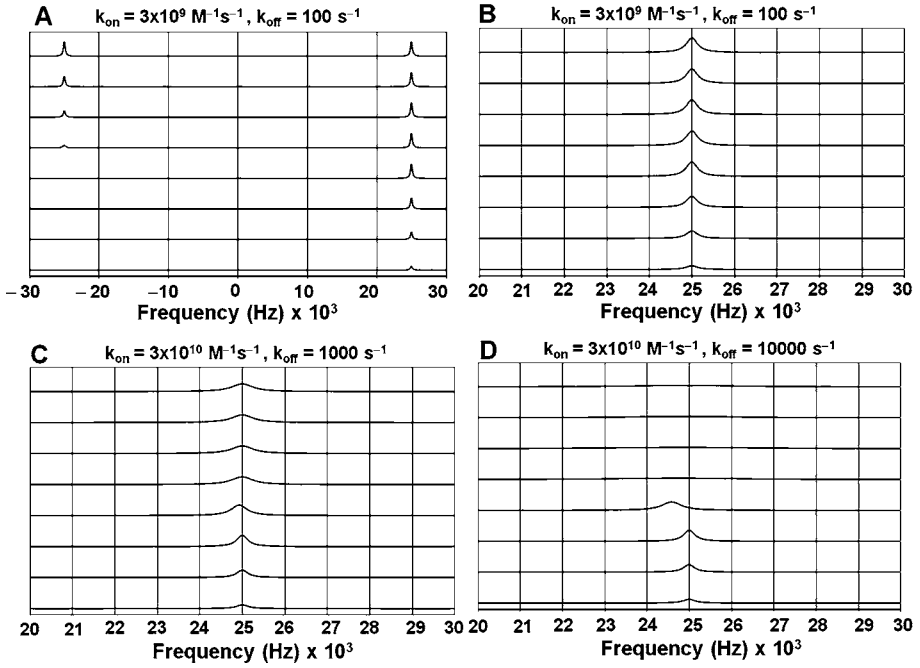

Figure 3. Results of two-site NMR titration simulations performed using eq 3 in Materials and Methods. The "bound" Cd(II) signal is shown at 25 000 Hz and the "free" Cd(II) signal is shown at −25 000 Hz ($\delta\nu$ = 450 ppm at 111 MHz). Both signals have R_2 = 1000 s^{-1} (line width = 318 Hz). The parameters chosen for these simulations are the following: (A) k_{on} = 3 × 10^9 M^{-1} s^{-1}, k_{off} = 100 s^{-1} (K_A = 3 × 10^7 M^{-1}). From bottom to top, the traces correspond to $[Cd]_{total}/[P]_{total}$ = 0.25, 0.50, 0.75, 1.00, 1.25, 1.50, 1.75, and 2.00 with $[P]_{total}$ = 4 mM (trimer). (B) An enlargement of the "bound" Cd(II) signal obtained from simulations in (A). (C) An enlargement of the "bound" Cd(II) signal of a simulation with k_{on} = 3 × 10^{10} M^{-1} s^{-1}, k_{off} = 1000 s^{-1} (K_A = 3 × 10^7 M^{-1}). Other parameters are the same as in (A). (D) An enlargement of the "bound" Cd(II) signal of a simulation with k_{on} = 3 × 10^{10} M^{-1} s^{-1}, k_{off} = 10 000 s^{-1} (K_A = 3 × 10^6 M^{-1}). Other parameters are the same as in (A).

studied show a well-defined ^{113}Cd(II) resonance around 550 ppm with a 300 Hz line width in the presence of substoichiometric amounts of ^{113}Cd(II) (Figure 2). The properties of these signals suggests a rigid, well-defined structure for bound ^{113}Cd(II). Indeed, the four-coordinate pseudotetrahedral CdS_3O environment has high symmetry; therefore, a small CSA and CSA broadening are to be expected.

The equilibrium constant K_A for the binding of Cd(II) to the Cys-substituted **Grand** peptides is >3 × 10^7 M^{-1}.[51] Based on the commonly quoted[52] maximum diffusion-limited bimolecular on-rate (k_{on}) of 3 × 10^{10} M^{-1} s^{-1}, one expects a maximum off-rate (k_{off}) <1000 s^{-1}. The predicted maximum off-rate is much smaller than the expected chemical shift difference of 3.5 × 10^6 rad s^{-1} between bound and free Cd(II) signal (500 ppm at 111 MHz). In agreement with the predicted slow-exchange regime, no chemical shift change was observed during the titration from substoichiometric to excess equivalents of ^{113}Cd-(II) (Figure 2). However, all spectra show increasing line broadening and decrease in intensity for the "bound" ^{113}Cd(II) signal when excess equivalents of ^{113}Cd(II) were added. The least amount of broadening and intensity change was observed for the site L12AL16C, while the largest amount of change was seen for site L26AL30C, both in the single site peptides (**Grand**L12AL16C, **Grand**L26AL30C) and in the dual site peptide (**Grand**L12AL16CL26AL30C). The signal intensity loss and progressive broadening is inconsistent with a two-site slow exchange mechanism. In a two-site slow exchange scheme, the intensity of the "bound" resonance should not change when excess free metal is present. In addition, the line width R_2/π of a "bound" resonance (when excess is present) is independent of the ratio metal free/bound and is determined by the intrinsic line width R_2^0/π at that site, augmented with the constant lifetime broadening k_{off}/π:

$$R_2/\pi = R_2^0/\pi + k_{off}/\pi \quad (10)$$

To demonstrate these points, and to explore the limits of the kinetic parameters, two-site chemical exchange simulations were carried out with parameters relevant to the experimental data, using the methods described in the Materials and Methods section. Figure 3A represents a classical slow exchange case. Using k_{on} = 3 × 10^9 M^{-1} s^{-1} and k_{off} = 100 s^{-1}, no shifts are observed for the "bound" signal over the titration regime. Also the exchange line broadening, as compared to the intrinsic line width of 300 Hz is minimal. In Figure 3C,D, the on-rate is increased up to the theoretical limit of 3 × 10^{10} M^{-1} s^{-1}, together with k_{off} = 1000 or 10 000 s^{-1}, respectively. The simulations now *do* show significant exchange broadening at supra-stoichiometic conditions. However, the broadening is *not progressive*, while the "bound" signal intensity remains constant (see Table 3). In addition, under these simulation conditions, significant chemical shifts changes for the "bound" signal are being observed, that are not observed in the experimental results.

Because of these simulated results, we conclude that a simple two-site exchange mechanism can at no choice of parameters account for the progressive broadening and intensity loss seen in the experimental data. Moreover, the best simulation with k_{off} = 10 000 s^{-1} starts to show intermediate exchange-induced chemical shift changes. Most problematic is the fact that the best simulation requires a very fast k_{on} = 3 × 10^{10} M^{-1} s^{-1}. Such a bimolecular on-rate is the *very* limit of diffusion control. According to collision theory, this fast rate is only reached when the entire surface of a macromolecule is involved in

dx.doi.org/10.1021/ja210510g | *J. Am. Chem. Soc.* 2012, 134, 6191−6203

Table 3. Simulated NMR Line Width of the "Bound Resonance" as a Function of the Ratio Ligand/Protein for Different Kinetic Models, Shown in Figures 3 and 7

	model			
	two-site	two-site	two-site	five-site
K_A^{app} (M^{-1})	3×10^7	3×10^7	3×10^6	3×10^7
k_{on} ($M^{-1}\,s^{-1}$)	3×10^9	3×10^{10}	3×10^{10}	complex
k_{off} (s^{-1})	100	1000	10 000	complex
R_2^{bound} (s^{-1})	1000	1000	1000	1000
$\delta\nu_{(free-bound)}$ (Hz)	50 000	50 000	50 000	50 000
	$\delta\nu_{1/2}{}^{bound}$ (Hz)			
ratio	two-site	two-site	two-site	five-site
0.25	318	318	318	318
0.5	318	318	318	318
0.75	318	318	318	318
1	330	500	1400	318
1.25	340	600	3000	414
1.5	340	600	3000	628
1.75	340	600	3000	1068
2	340	600	3000	2100

capturing a substrate, followed by surface diffusion which funnels the substrate into an *exposed* active site.[52,53] In comparison, for the present case, it is quite improbable that the collision rate could be the rate-limiting step. After all, the Cd(II) needs to bind to an *interior* site located at the center of the three-helix bundle. Much more likely, one expects that a much slower transient unfolding or breathing process, which would allow access of Cd(II) to the interior, is rate limiting.

Formulation of a Multisite Exchange Model. At this point one can conclude that the NMR titration data are incompatible with a simple two-site exchange scheme because at supra-stoichiometric ratios the signal corresponding to the "bound" state loses intensity and it broadens progressively. Several thermodynamic models can be proposed that can account for the reduction of the NMR signals at supra-stoichiometric ratios. A satisfactory model is high-affinity metal binding in the primary binding site in species Q, followed by low-affinity binding in an auxiliary site *which changes the properties of the primary binding site* as shown in Figure 4. If we choose the equilibrium binding constant $K_{PQ} = k_{PQ}/k_{QP}$ in Figure 4 to be larger than $K_{PR} = k_{PR}/k_{RP}$ then species Q will disappear when the Cd(II) concentration is increased in excess of stoichiometry with a subsequent increase in the population of the species S. In this model, one will observe the disappearance of the signal with NMR properties β when the metal concentration is increased in excess of stoichiometry. Reasons why the signal of site δ of species S may be undetectable will be discussed below. Invoking this multisite exchange scheme, the concentrations of the different species in Figure 4 were computed as a function of the ratio of metal/protein concentrations using numerical methods as described in the Material and Methods. With a choice of the equilibrium association constants $K_{PQ} = K_{RS} = 3 \times 10^7\ M^{-1}$ (primary binding site), and $K_{PR} = K_{QS} = 10^4\ M^{-1}$ (secondary binding site), the profile as shown in Figure 5 is obtained. The results from these simulations show that this scheme allows for disappearance of the species Q, because it is being displaced by the species S. Hence, this multisite exchange scheme can account for the hallmark effect observed in the experimental titrations: the bound Cd(II) signal loses intensity when excess Cd(II) is present.

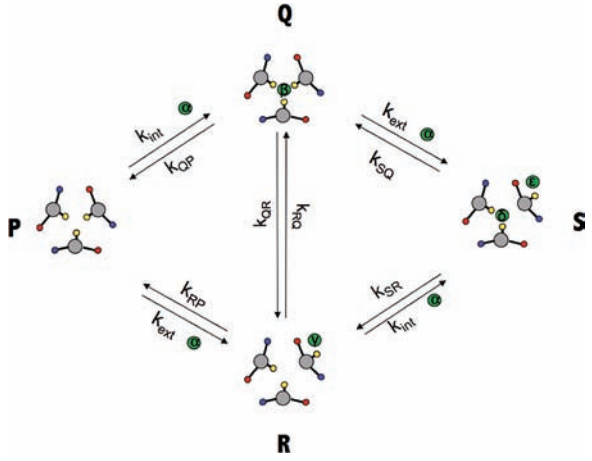

Figure 4. Cartoon representation of the model containing two metal binding sites. The scheme has five thermodynamic "species", P, Q, R, S, and free metal Cd(II). The scheme has five NMR species α, β, γ, δ, and ε. The direct communication between species Q and R ("Cd(II) internalization") is important for the kinetics of metal binding but is thermodynamically irrelevant. In the cartoons, Cd(II) is represented as a green circle, Cys-SH groups as yellow circles, Glu-COO^- groups as red circles, and Lys NH_3^+ groups as blue circles.

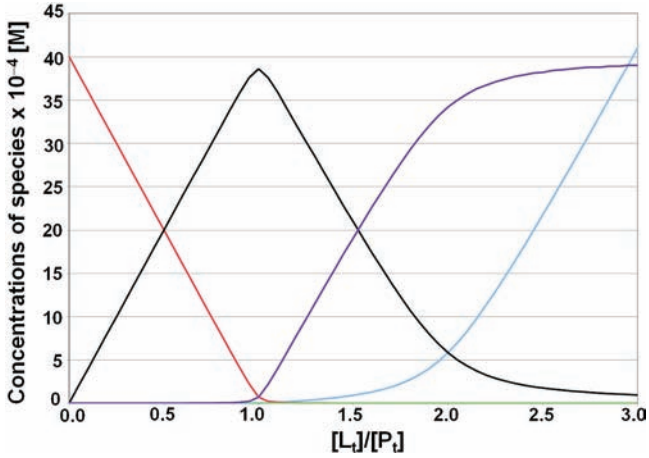

Figure 5. Equilibrium concentrations of different species obtained after 5 s of kinetic simulations as a function of total metal concentration. This simulation time is 50 times longer than it is needed to reach equilibrium (see Figure S9). $[Cd]_{free}$ is red; [P] is cyan; [Q] is black; [R] is green; [S] is purple. Simulation conditions: Total protein concentration 4 mM (trimer); $k_{PQ} = k_{RS} = k_{int} = 3 \times 10^5\ M^{-1}\,s^{-1}$; $k_{QP} = k_{SR} = 0.01\ s^{-1}$; $k_{PR} = k_{QS} = k_{ext} = 10^7\ M^{-1}\,s^{-1}$; $k_{RP} = k_{SQ} = 10^3\ s^{-1}$, $k_{RQ} = 10^3\ s^{-1}$, $k_{QR} = 0.333\ s^{-1}$ (corresponding to the equilibrium association constants $K_{PQ} = 3 \times 10^7\ M^{-1}$ and $K_{PR} = 10^4\ M^{-1}$).

In order to also account for the progressive increase in line width of the "bound" resonance (see Table 2), the "species" scheme of Figure 4 must be translated into a "site" scheme for the Cd(II) ion as shown in Figure 6. The scheme in Figure 4 corresponds to a five-site chemical exchange scheme. According to this scheme Cd(II) can be free (denoted as site α), bound to site β in species Q, bound to site γ in species R, or bound to sites δ or ε in species S. Potentially, all five sites have different NMR parameters. That is, the primary metal binding site β may change in frequency and line width if excess metal binds to the auxiliary site in species S (i.e., sites β and δ are different for NMR).

dx.doi.org/10.1021/ja210510g | J. Am. Chem. Soc. 2012, 134, 6191−6203

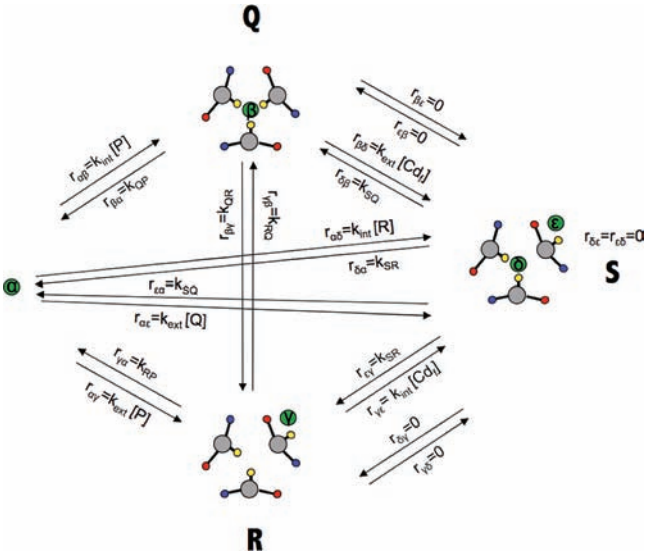

Figure 6. Five-site NMR exchange parameters for the metal in the scheme of Figure 4. In the cartoons, Cd(II) is a green circle, Cys-SH groups are yellow circles, Glu-COO^- groups are red circles, and Lys NH_3^+ groups are blue circles. The relevant exchange rates are related to the kinetic constants in Figure 4 as indicated. (Also see eqs 8 and 9 and Tables S1 and S2 of the SI.)

The exchange rates between the sites are related to the kinetic constants in Figure 4 and the concentrations of the different species [P], [R],[Q], [S], and free [Cd] as indicated in Figure 6 and eqs 7 and 8 in the Materials and Methods section. In the simulations, it was assumed that no *direct* exchange can occur between the internal and external sites δ and ε in species S because the sites are occupied. It was also assumed that the internal site β cannot directly interchange with the external site ε and that the external site γ cannot directly interchange with the internal site δ, because these processes would require coordinated rearrangement and binding/release of two Cd(II) ions. The possibility that external Cd(II) in species R (site γ) can become internalized in species Q (site β) was allowed in the computations. While this internalization process does not change the thermodynamics (all is balanced in Carnot cycles), or the NMR line widths (see SI), it forms a realistic pathway for the binding of Cd(II) to the internal site (discussed below).

The detailed-balanced equilibrium kinetic site−site exchange parameters were inserted into five-site chemical exchange BMC equations shown in eqs 7 and 8 in the Materials and Methods. The equations were numerically integrated with the equilibrium concentrations of the different species as starting conditions, listed in Tables S1 and S2 of the SI. The parameters chosen correspond to slow exchange for all sites. The obtained FIDs were Fourier transformed yielding the spectra shown in Figure 7. Figure 7A corresponds to a slight excess of Cd(II). The resonances for all sites are seen, except for site γ in species R which is too small in intensity. Figure 7B shows a zoom in on the "bound" signal (site β in species Q) as a function of the Cd(II)/peptide ratio. The simulated spectra correspond very closely to the experimental NMR data for site L26AL30C, both in the single (**Grand**L26AL30C) and dual site (**Grand**-L12AL16CL26AL30C) peptides (Figure 2B,C). As is documented in Table 3, the line width of the "bound" resonance increases as the excess Cd(II) is increased. This progressive broadening, consistent with the experimental data, is caused by *increasing* lifetime broadening of site β in species Q, because it

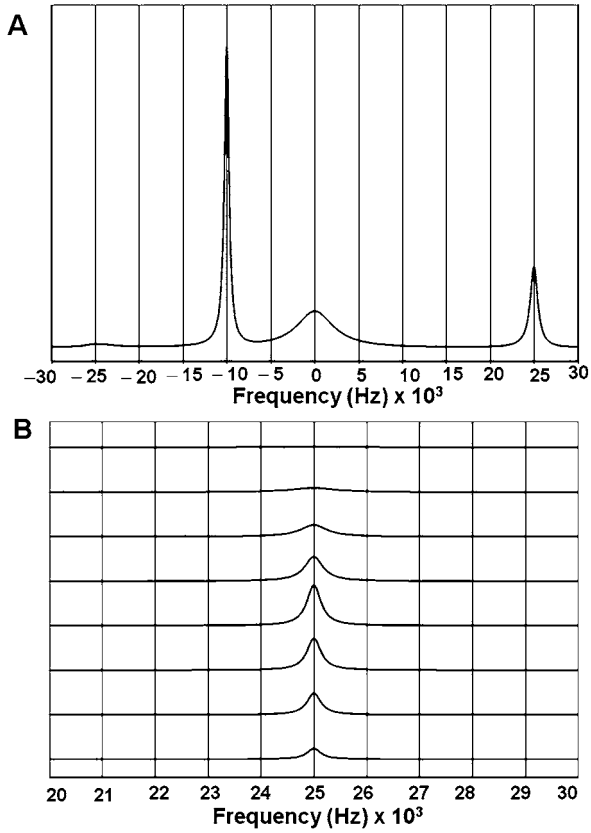

Figure 7. Simulation results of the five-site exchange NMR spectra according to the model represented in Figure 6 and using eqs 8 and 9. Site α (free Cd(II)) resonates at −25 000 Hz; site β (the "primary" buried site in species Q) at +25 000 Hz; site γ (the surface site in species R) at −15 000 Hz (concentration too low to be visible); site δ (the buried site in species S) at 0 Hz; site ε (the surface site in species S) at −10 000 Hz. All sites have R_2 = 1000 s^{-1}. Site−site exchange rates were derived from the rates in Figure 4, as indicated in Figure 6 with values as listed in the legend of Figure 5 and Tables S1 and S2 of the SI. (A) Total protein concentration = 4 mM (trimer); total ligand concentration = 9.0 mM. (B) Simulation results obtained for different ratios of $[Cd]_{total}/[P]_{total}$. Only the signal for site β (the buried site in species Q) at +25 000 Hz is shown. From bottom to top the traces are obtained using the following ratios: $[Cd]_{total}/[P]_{total}$ = 0.25, 0.50, 0.75, 1.00, 1.25, 1.50, 1.75, and 2.00, with $[P]_{total}$ = 4 mM (trimer).

is *converted* to site δ in species S, with an *increasing* rate depending on the concentration of free Cd(II):

$$\frac{1}{\tau\beta} = k_{QP} + k_{QR} + k_{ext}[Cd]_{free} \quad (11)$$

It thus appears that the simple model of Figure 4, representing five-site metal exchange, can account for both the decrease in intensity of the bound signal and the progressive line broadening when excess free Cd(II) is present.

Why the other lines are not observed in the experiment may be understood as follows. As we already know, the signal of ^{113}Cd(II) ion in water is broadened beyond detection. Hence, it may be expected that the Cd(II) signals of the solvent-exposed sites γ and ε are also broadened away. The Cd(II) signal of internal site δ in structure S is invisible because we associate this structure with a destabilized bis-liganded internal Cd(II). Such a destabilization likely causes excessive exchange broadening of the signal. Moreover, ^{113}Cd(II) is also known to the have a large chemical shift anisotropy, which can reach to 100 ppm

dx.doi.org/10.1021/ja210510g | *J. Am. Chem. Soc.* 2012, 134, 6191−6203

in asymmetric environments such as this site.[50] The associated line broadening effects, especially at higher magnetic fields, would further exacerbate the broadening of Cd(II) in the site δ in species S. While the allosteric/kinetic/NMR model contains many parameters, only k_{int}, (the bimolecular on-rate to the internal site) and k_{RP} (the off-rate of the external site) can be freely chosen—with all other parameters being restrained by the overall experimental affinity and by the observed experimental line-broadening.

Nature of the Additional Cadmium(II) Binding Site(s). The three-stranded coiled-coil peptides have been designed as repeating heptads LKALEEK, with a hydrophobic core formed by residues in positions 1 and 4. The Glu residues located at the fifth position are involved in interhelical electrostatic interactions with the Lys residues located at the seventh position. These electrostatic interactions are essential for the formation of stable trihelical coiled coils. From our previous studies we know that the peptides containing four heptads or more (**TRI**, **GRAND**, and **Coil Ser**) exist as parallel three-stranded coiled coils even in the absence of metals at any pH higher than 5.5.[25,30,47,48] Species Q in Figure 4 represents the situation where Cd(II) is bound to three cysteines at the interior of the three-stranded coiled coils under stoichiometric conditions. The analysis of the NMR data leads to the prediction that Cd(II) must also bind elsewhere, and that this external binding affects the Cd(II) bound to three cysteines at the interior. It is quite reasonable to hypothesize that the Glu residues can also bind to Cd(II), and that this binding interferes with the overall stability of the peptide and consequently with the NMR signal of the Cd(II) bound to the internal site.

To test whether Glu residues are involved in Cd(II) binding, Glu 28, located closest in sequence to the metal binding Cys residue at position 30, was mutated to Gln. The resulting peptide is **Grand**L26AE28QL30C. Aliquots of ^{113}Cd(II) were added to a solution containing 3.7 mM (**Grand**L26AE28QL30C)$_3$ at pH 8.5 and the NMR spectral changes were monitored. In the presence of 1.0 equiv of ^{113}Cd(II), a single sharp resonance with a chemical shift of 587 ppm was observed (Figure 8, and Figure S8 of the SI). The ^{113}Cd NMR resonance at 587 ppm broadened slowly with increasing amounts of ^{113}Cd(II) and was broadened beyond detection in the presence of 2.1 equiv of ^{113}Cd(II), which is a significantly larger ratio of Cd(II)/(peptide)$_3$ than what was needed for the complete broadening of the NMR signal for the **Grand**L26AL30C peptide. The resonance for the latter peptide was completely broadened beyond detection in the presence of 1.7 equiv of ^{113}Cd(II) (Figure 2B). We conclude that the effects seen on the kinetics of the internal Cd(II) by mutagenesis of a neighboring external Glu, support the hypothesis that the Glu residues are involved in excess Cd(II) binding.

Functional Interpretation of the Multisite Cadmium(II) Binding. The inferred presence of an external Cd(II) binding site leads to a model how an external binding site may be essential to the Cd(II) binding process to the primary site itself. The model has been represented as cartoons for the different states in Figures 4 and 6. In the model, we envision that Cd(II) is initially coordinated by the Glu residue(s) at the surface (red circles) located closest to the metal binding Cys residues (yellow circles) in species R. As suggested by the data discussed above, this leads to destabilization of the Glu-Lys (blue circle) interaction which in turn would facilitate the sequestration of the metal in the interior. This model is attractive as it can account for relatively fast Cd(II) binding to

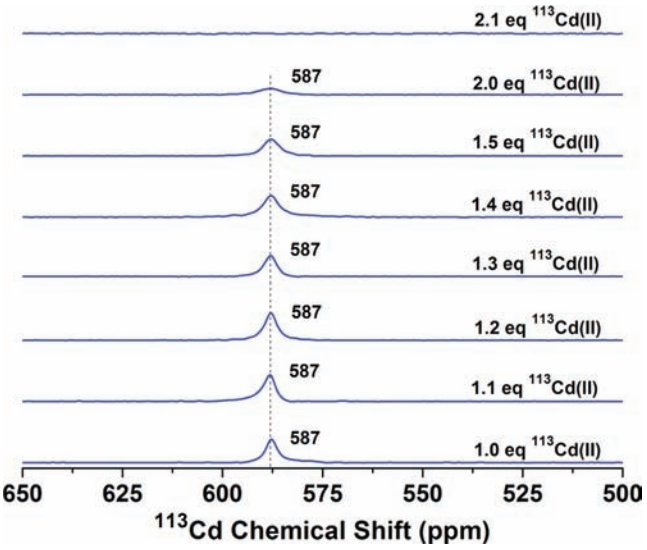

Figure 8. ^{113}Cd NMR spectra of a solution containing 3.7 mM of the mutant protein (**Grand**L26AE28QL30C)$_3$ at pH 8.5 with different equivalents of added ^{113}Cd(NO$_3$)$_2$. In this mutant the Glu 28, located close to the primary metal binding Cys site in **Grand**L26AL30C peptide was replaced by Gln to test the hypothesis whether any surface Glu residue(s) initially coordinate to the Cd(II) ion. The results from this experiment show that Cd(II)-induced line broadening is attenuated compared to the **Grand**L26AL30C peptide, indicating that Glu 28 does play a role in Cd(II) exchange.

the internal binding site as a two-step sequential process involving species R and Q. Figures S9 and S10 of the SI show the time courses of the simulated binding kinetics according to the model of Figure 4, starting with unbound Cd(II) and unbound protein. Indeed, one observes that species R becomes rapidly and transiently populated before species Q becomes populated. We believe that this model may also be of relevance for metal binding to naturally occurring proteins.

Although not essential to the sequential binding model, we also propose the *nature* of this destabilized state which is corroborated by X-ray structures of related metal binding peptides (Coil Ser), where the Cys side chains can adopt multiple conformations partitioned between the helical interior and toward the helical interface.[47,48] The Cys sulfur oriented toward the helical interface helps to coordinate the external Cd(II) ion initially. This situation is symbolized as species R in Figures 4 and 6, where the Cd(II) is coordinated by Glu and one of the external Cys residues. Next, a rotation of Cys side chains followed by breathing of the helices are thought to internalize the surface-bound Cd(II) to the interior (species S in Figures 4 and 6), where the Cd(II) at the interior is coordinated by just two Cys thiolates. The latter situation is supported by an X-ray structure of a Coil Ser peptide where one Hg(II) ion is bound to two thiols of Pen as linear HgS_2 at the interior of the coiled coil, whereas another Hg(II) is present at the helical interface and coordinated to a Glu and a Pen side chain oriented toward the helical interface (Zastrow, M., Pecoraro, V. L., unpublished results).

Comparison of Metal Exchange between Three- and Four-Coordinate Cadmium(II) Centers. Based on the above discussion we have established that Cd(II) insertion to peptides as four-coordinate CdS_3O structures are highly intricate in nature involving auxiliary surface residues (Glu) in addition to the primary binding site (Cys) at the polypeptide interior.

dx.doi.org/10.1021/ja210510g | J. Am. Chem. Soc. 2012, 134, 6191−6203

We have also proposed a mechanism by which the surface-bound Cd(II) can be internalized. As a final note, we investigated the peptide **Grand**L16PenL19IL23PenL26I, which binds Cd(II) ions as three-coordinate CdS_3 structures.[37] Figures S11 and S12 of the SI show that, unlike the behavior for CdS_3O centers, the addition of excess ^{113}Cd(II) does not cause line broadening to either of the resonances with chemical shifts 681 and 686 ppm. The Pen and Ile residues in the **Grand**L16PenL19IL23PenL26I peptide provide improved packing conferring higher stability to the coiled-coil assembly,[37] making the three-coordinate Cd(II) sites more rigid and compact. Further, the additional methyl groups on the Pen ligand are expected to inhibit, in this very well packed structure, rotation of the sulfur ligand toward the helical interface. In the **Grand**L12AL16CL26AL30C peptide, on the other hand, each Leu substitution to Cys or Ala results in a loss of free energy of ∼4 kcal/mol,[37] making this an inherently less stable construct compared to the **Grand**-L16PenL19IL23PenL26I peptide.

CONCLUSIONS

In this work we have investigated the exchange of cadmium(II) into *de novo* designed three-stranded coiled-coil peptides that contain both dual and single metal binding sites using ^{113}Cd NMR spectroscopy and mathematical simulations. Chemical exchange kinetics of Cd(II) is observed when the metal ion is bound as a four-coordinate CdS_3O structure in pseudotetrahedral geometry. The exchange of Cd(II) occurs on the slow exchange regime but is incompatible with a simple two-site exchange mechanism. The experimental NMR data are explained by formulating a multisite binding model which involves coordination of Cd(II) to surface glutamates, a process which destabilizes the primary Cd(II) binding site (cysteines) at the interior. The model also provides a general kinetic mechanism for the insertion of metals from the polypeptide surface to the internal binding sites, with likely applications to more complex biological metal-binding proteins. Due to fraying of the coiled coils at the ends, the L26AL30C site, located proximal to the helical terminus, is more susceptible to destabilization by external metal binding as compared to the L12AL16C located almost in the middle of the helix. These differences demonstrate that the dynamics of metal binding and exchange can be significantly different, depending on the location of the metal site within a specified secondary structure. Finally, the three-coordinate trigonal planar CdS_3 structures exchange too slowly to be monitored by ^{113}Cd NMR spectroscopy.

ASSOCIATED CONTENT

Supporting Information

Results from UV−vis spectroscopy; part of the NMR discussion; parameters for fitting the five-site exchange data; UV−vis titration of Cd(II) to **Grand**L26AE28QL30C, **Grand**-L12AL16C, and **Grand**L26AL30C; pH dependence of Cd(II) binding to **Grand**L26AE28QL30C; ^{113}Cd NMR spectra of **Grand**L16PenL19IL23PenL26I in the presence of different equivalents of ^{113}Cd(II); spectra with full scale of ^{113}Cd NMR chemical shifts for **Grand**L12AL16C and **Grand**L26AL30C; simulated binding kinetics of Cd(II) according to eqs 5; and fittings of ^{113}Cd NMR spectra for **Grand**L12AL16C, **Grand**L26AL30C, **Grand**L12AL16CL26AL30C, **Grand**-L26AE28QL30C, and **Grand**L16PenL19IL23PenL26I. This material is available free of charge via the Internet at http://pubs.acs.org.

AUTHOR INFORMATION

Corresponding Author

vlpec@umich.edu; zuiderwe@umich.edu

Present Address

[‖]Department of Chemistry, School of Chemical Sciences, University of Illinois at Urbana−Champaign, 600 S. Mathews Ave., Urbana, IL 61801

Notes

The authors declare no competing financial interest.

ACKNOWLEDGMENTS

V.L.P. thanks the National Institutes of Health for support of this research (ES012236). O.I. thanks the Margaret and Herman Sokol Foundation for a Postdoctoral Award. E.R.P.Z. most gratefully thanks the Department of Biological Chemistry of the University of Michigan Medical School for continued support.

REFERENCES

(1) Masuoka, J.; Saltman, P. *J. Biol. Chem.* **1994**, *269*, 25557−25561.
(2) Means, A. R.; Dedman, J. R. *Nature* **1980**, *285*, 73−77.
(3) Rosenzweig, A. C.; O'Halloran, T. V. *Curr. Opin. Chem. Biol.* **2000**, *4*, 140−147.
(4) Xia, W.; Li, H.; Sze, K.-H.; Sun, H. *J. Am. Chem. Soc.* **2009**, *131*, 10031−10040.
(5) Rosenzweig, A. C. *Acc. Chem. Res.* **2000**, *34*, 119−128.
(6) O'Halloran, T. V.; Culotta, V. C. *J. Biol. Chem.* **2000**, *275*, 25057−25060.
(7) Wernimont, A. K.; Huffman, D. L.; Lamb, A. L.; O'Halloran, T. V.; Rosenzweig, A. C. *Nat. Struct. Biol.* **2000**, *7*, 766−771.
(8) Wright, J. G.; Natan, M. J.; MacDonnell, F. M.; Ralston, D. M.; O'Halloran, T. V. *Prog. Inorg. Chem.: Bioinorg. Chem.* **1990**, *38*, 323−412.
(9) Wright, J. G.; Tsang, H.-T.; Penner-Hahn, J. E.; O'Halloran, T. V. *J. Am. Chem. Soc.* **1990**, *112*, 2434−2435.
(10) Ye, J.; Kandegedara, A.; Martin, P.; Rosen, B. P. *J. Bacteriol.* **2005**, *187*, 4214−4221.
(11) Banci, L.; Bertini, I.; Cantini, F.; Ciofi-Baffoni, S.; Cavet, J. S.; Dennison, C.; Graham, A. I.; Harvie, D. R.; Robinson, N. J. *J. Biol. Chem.* **2007**, *282*, 30181−30188.
(12) Busenlehner, L. S.; Weng, T.-C.; Penner-Hahn, J. E.; Giedroc, D. P. *J. Mol. Biol.* **2002**, *319*, 685−701.
(13) Busenlehner, L. S.; Cosper, N. J.; Scott, R. A.; Rosen, B. P.; Wong, M. D.; Giedroc, D. P. *Biochemistry* **2001**, *40*, 4426−2236.
(14) Shi, W.; Dong, J.; Scott, R. A.; Ksenzenko, M. Y.; Rosen, B. P. *J. Biol. Chem.* **1996**, *271*, 9291−9297.
(15) Sun, Y.; Wong, M.; Stalhandske, C.; Scott, R. A.; Rosen, B. P. *FASEB J.* **1999**, *13*, A1464−A1464.
(16) Borremans, B.; Hobman, J. L.; Provoost, A.; Brown, N. L.; van der Lelie, D. *J. Bacteriol.* **2001**, *183*, 5651−5658.
(17) Lamb, A. L.; Torres, A. S.; O'Halloran, T. V.; Rosenzweig, A. C. *Biochemistry* **2000**, *39*, 14720−14727.
(18) Lamb, A. L.; Torres, A. S.; O'Halloran, T. V.; Rosenzweig, A. C. *Nat. Struct. Biol.* **2001**, *8*, 751−755.
(19) Lamb, A. L.; Wernimont, A. K.; Pufahl, R. A.; O'Halloran, T. V.; Rosenzweig, A. C. *Nat. Struct. Biol.* **1999**, *6*, 724−729.
(20) Huffman, D. L.; O'Halloran, T. V. *J. Biol. Chem.* **2000**, *275*, 18611−18614.
(21) Tosha, T.; Ng, H.-L.; Bhattasali, O.; Alber, T.; Theil, E. C. *J. Am. Chem. Soc.* **2010**, *132*, 14562−14569.
(22) Theil, E. C. *Annu. Rev. Biochem.* **1987**, *56*, 289−315.
(23) Bryson, J. W.; Betz, S. F.; Lu, Z. X.; Suich, D. J.; Zhou, H. X.; O'Neil, K. T.; DeGrado, W. F. *Science* **1995**, *270*, 935−941.
(24) Dieckmann, G. R.; McRorie, D. K.; Tierney, D. L.; Utschig, L. M.; Singer, C. P.; O'Halloran, T. V.; Penner-Hahn, J. E.; DeGrado, W. F.; Pecoraro, V. L. *J. Am. Chem. Soc.* **1997**, *119*, 6195−6196.

(25) Dieckmann, G. R.; McRorie, D. K.; Lear, J. D.; Sharp, K. A.; DeGrado, W. F.; Pecoraro, V. L. *J. Mol. Biol.* **1998**, *280*, 897−912.
(26) Pecoraro, V. L.; Peacock, A. F. A.; Iranzo, O.; Luczkowski, M. *Bioinorganic Chemistry*; American Chemical Society: Washington, DC, 2009; pp 183−197, SE-112.
(27) Iranzo, O.; Thulstrup, P. V.; Ryu, S.-B.; Hemmingsen, L.; Pecoraro, V. L. *Chem.—Eur. J.* **2007**, *13*, 9178−9190.
(28) Dieckmann, G. R. Ph.D. Thesis, University of Michigan (Ann Arbor), **1995**.
(29) Farrer, B.; McClure, C.; Penner-Hahn, J. E.; Pecoraro, V. L. *Inorg. Chem.* **2000**, *39*, 5422−5423.
(30) Touw, D. S.; Nordman, C. E.; Stuckey, J. A.; Pecoraro, V. L. *Proc. Natl. Acad. Sci. U.S.A.* **2007**, *104*, 11969−11974.
(31) Lee, K.-H.; Cabello, C.; Hemmingsen, L.; Marsh, E. N. G.; Pecoraro, V. L. *Angew. Chem., Int. Ed.* **2006**, *45*, 2864−2868.
(32) Hemmingsen, L.; Narcisz, K.; Danielsen, E. *Chem. Rev.* **2004**, *104*, 4027−4061.
(33) Matzapetakis, M.; Farrer, B. T.; Weng, T.-C.; Hemmingsen, L.; Penner-Hahn, J. E.; Pecoraro, V. L. *J. Am. Chem. Soc.* **2002**, *124*, 8042−8054.
(34) Lee, K. H.; Matzapetakis, M.; Mitra, S.; Marsh, E. N. G.; Pecoraro, V. L. *J. Am. Chem. Soc.* **2004**, *126*, 9178−9179.
(35) Peacock, A. F. A.; Hemmingsen, L.; Pecoraro, V. L. *Proc. Natl. Acad. Sci. U.S.A.* **2008**, *105*, 16566−16571.
(36) Iranzo, O.; Cabello, C.; Pecoraro, V. L. *Angew. Chem., Int. Ed.* **2007**, *46*, 6688−6691.
(37) Iranzo, O.; Chakraborty, S.; Hemmingsen, L.; Pecoraro, V. L. *J. Am. Chem. Soc.* **2011**, *133*, 239−251.
(38) Ghosh, D. Ph.D. Thesis, University of Michigan (Ann Arbor), **2006**.
(39) Chan, W. C.; White, P. D. *Fmoc Solid Phase Peptide Synthesis: A Practical Approach*; Oxford Univ. Press: New York, 2000.
(40) Farrer, B. T.; Harris, N. P.; Balchus, K. E.; Pecoraro, V. L. *Biochemistry* **2001**, *40*, 14696−14705.
(41) Mantle, M.; Stewart, G.; Zayas, G.; King, M. *Biochem. J.* **1990**, *266*, 597−604.
(42) Matzapetakis, M.; Ghosh, D.; Weng, T.-C.; Penner-Hahn, J. E.; Pecoraro, V. L. *J. Biol. Inorg. Chem.* **2006**, *11*, 876−890.
(43) Iranzo, O.; Lee, K. H.; Jakusch, T.; Hemmingsen, L.; Pecoraro, V. L. *Chem.—Eur. J.* **2009**, *15*, 3761−3772.
(44) Cobas, C.; Cruces, J.; Sardina, F. J. *MestRe-C*, 2.3 ed.; Universidad de Santiago de Compostela: Spain, 2000.
(45) Cavanagh, J.; Fairbrother, W. J.; Palmer III, A. G.; Skelton, N. J. Academic Press Inc., San Diego, **1996**; p 279.
(46) Summers, M. F. *Coord. Chem. Rev.* **1988**, *86*, 43−134.
(47) Peacock, A. F. A.; Stuckey, J. A.; Pecoraro, V. L. *Angew. Chem., Int. Ed.* **2009**, *48*, 7371−7374.
(48) Chakraborty, S.; Touw, D. S.; Peacock, A. F. A.; Stuckey, J.; Pecoraro, V. L. *J. Am. Chem. Soc.* **2010**, *132*, 13240.
(49) Lovejoy, B.; Choe, S.; Cascio, D.; McRorie, D.; DeGrado, W.; Eisenberg, D. *Science* **1993**, *259*, 1288−1293.
(50) Tinet, D.; Faugere, A. M.; Prost, R. *J. Phys. Chem.* **1991**, *95*, 8804.
(51) Ghosh, D.; Lee, K.-H.; Demeler, B.; Pecoraro, V. L. *Biochemistry* **2005**, *44*, 10732−10740.
(52) Alberty, R. A.; Hammes, G. G. *J. Phys. Chem.* **1958**, *62*, 154.
(53) Zhou, G.; Wong, M.; Zhou, G. *Biophys. Chem.* **1983**, *18*, 125.